

# OVIP: ONLINE VISION-LANGUAGE PREFERENCE LEARNING FOR VLM HALLUCINATION

**Shujun Liu**  
Fudan University

**Siyuan Wang**  
University of Southern California

**Zejun Li**  
Fudan University

**Jianxiang Wang**  
ByteDance

**Cheng Zeng**  
ByteDance

**Zhongyu Wei**  
Fudan University

## ABSTRACT

Large vision-language models (LVLMs) remain vulnerable to hallucination, often generating content misaligned with visual inputs. Although recent training-based approaches aim to mitigate hallucination, they typically rely on predefined or randomly edited negative samples that do not reflect actual model errors, thus limiting training efficacy. In this work, we propose an Online Vision-language Preference Learning (OVIP) framework that dynamically constructs contrastive training data based on the model’s own hallucinated outputs. By identifying semantic differences between sampled response pairs and synthesizing negative images using a diffusion model, OViP generates more relevant supervision signals in real time. This failure-driven training enables adaptive alignment of both textual and visual preferences. Moreover, we refine existing evaluation protocols to better capture the trade-off between hallucination suppression and expressiveness. Experiments on hallucination and general benchmarks demonstrate that OViP not only reduces hallucinations while preserving core multi-modal capabilities, but also substantially improves training efficiency. Code is available at <https://github.com/lsjlsj35/Online-Vision-Language-Preference-Learning-for-VLM-Hallucination>.

## 1 INTRODUCTION

Large vision-language models (LVLMs) (Alayrac et al., 2022; Chen et al., 2023; 2024a; Liu et al., 2023; 2024b) have demonstrated remarkable performance across a wide range of multi-modal tasks (Dai et al., 2023; Li et al., 2023a; Bai et al., 2023; Wang et al., 2024b) by integrating pre-trained visual encoders with large language models (LLMs) to process and generate language grounded in visual inputs. However, LVLMs continue to struggle with persistent hallucination issues (Li et al., 2023b; Bai et al., 2024), often exhibiting incorrect references to visual content (Liu et al., 2024a; Zhou et al., 2023; Bai et al., 2024). These errors manifest as misattributing object properties, describing nonexistent entities, or fabricating spatial relationships that do not align with the image. Such inconsistencies undermine the model’s faithfulness to the input and hinder further reasoning capabilities, significantly limiting the reliability of LVLMs in real-world applications.

Recent success of Direct Preference Optimization (DPO) (Rafailov et al., 2023) in LLMs alignment has inspired the exploration of multi-modal DPO to mitigate hallucination in LVLMs (Yu et al., 2024a;b; Xie et al., 2024; Sarkar et al., 2024). However, early efforts directly extend the original DPO designs from LLMs to LVLMs by constructing preference pairs solely on textual responses given the same image input, primarily focusing on response-side preference optimization and showing limited effectiveness. Recent advancements incorporate additional preference pairs conditioned on varying image inputs while keeping the same response, optimizing both visual and textual preference optimization (Wang et al., 2024a; Wu et al., 2025; Fu et al., 2025). This paradigm provides a complementary training signal that encourages the model to attend more closely to visual content.

Please contact us at [shujuanliu24@m.fudan.edu.cn](mailto:shujuanliu24@m.fudan.edu.cn).

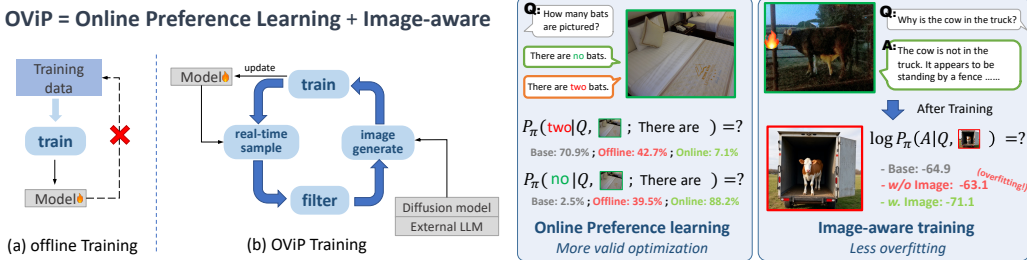


Figure 1: Offline training (a) relies on static, predefined datasets and fails to adapt to the model’s evolving failure patterns, limiting its ability to address hallucinations effectively. Moreover, neglecting the role of visual input will result in overfitting to language priors. In contrast, OViP (b) combines online preference learning with image-aware training in a unified framework, enabling real-time data construction grounded in model behavior.

However, prior work mainly relies on existing paired datasets (Wu et al., 2025) or expert-defined patterns to construct negative image inputs, using techniques such as random cropping (Wang et al., 2024a), noise disruption (Zhou et al., 2024a), object removal (Lu et al., 2025), or human/LLMs generated element-replaced response for image editing (Xie et al., 2024). These strategies are typically not explicitly tied to model failures, resulting in distribution misalignment between the generated negatives and the model’s actual hallucination behavior, thereby offering limited improvement and failing to support adaptive and continual online<sup>1</sup> learning (Guo et al., 2024). To address these limitations, we propose a failure-guided negative generation strategy that directly targets self-generated hallucinated responses, enabling the real-time creation of more in-distribution counterexamples through text-to-image generation. Specifically, we sample and filter positive and negative response pairs from the model’s textual outputs. Then we employ LLMs to generate an image prompt based on the negative response, particular emphasizing its differences from the positive response, and subsequently synthesize the corresponding negative image using a diffusion model (Zhang et al., 2023).

Building upon this negative generation strategy, we further introduce an online vision-language preference learning framework (OViP) on both response and image sides, to dynamically construct and learn from preference data during training. Similar to reinforcement learning paradigms, OViP samples LVLMs’ outputs throughout the training process and creates both response-centric and image-centric preference pairs in real time. As illustrated in Figure 1, these dual signals supervise the model to generate outputs more faithfully grounded in visual content. By continuously sampling and integrating new preference pairs based on emerging failure patterns, OViP enables adaptive learning that aligns with the evolving output distributions of the LVLMs. This ongoing adaptation mitigates the limitations of static datasets and reduces the reliance on extensive manual curation.

We evaluate our framework on diverse multi-modal benchmarks, covering both hallucination-focused and general tasks. Based on our experiments, we find a notable trade-off between hallucination suppression and general capability or informativeness (what we refer to as “implicit hallucination”). To address this, we refine existing evaluation protocols and reveal that many prior methods tend to overestimate their improvements. Experimental results show that OViP delivers significant advantages in both performance and efficiency. Furthermore, we investigate the role of online training and visual signals, as well as their interactions, in shaping training effectiveness.

## 2 METHODOLOGY

In this section, we first provide an overview of the Online Vision-Language Preference Learning (OViP) framework (Section 2.1). We then elaborate the process of constructing the online preference pairs during training (Section 2.2) followed by how to learn from these preference data (Section 2.3).

<sup>1</sup>We adopt the LLM community’s convention of using “online” to denote “on-policy” in RL.

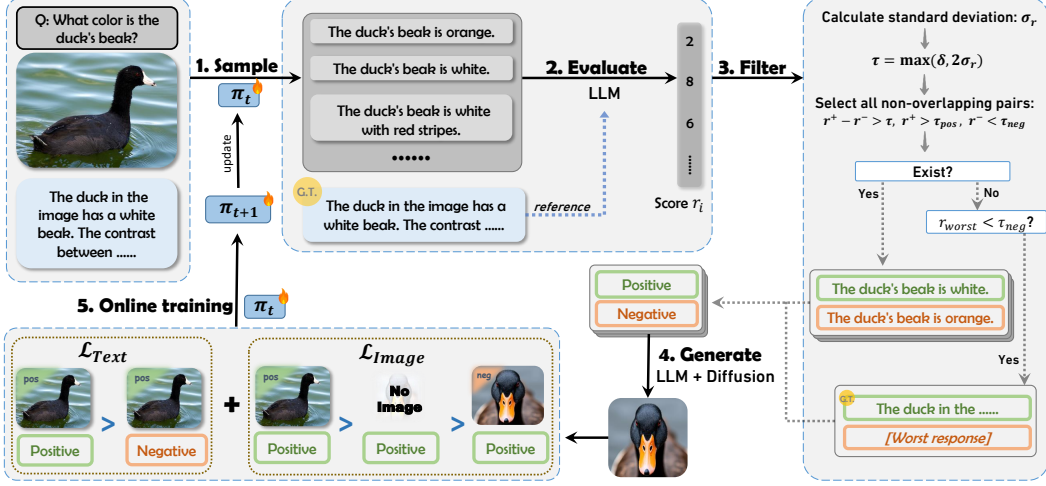


Figure 2: Overview of OViP. Given an image and a query, we employ the current model  $\pi_t$  to generate multiple responses, which are then evaluated by an external LLM with reference to the ground truth. We filter and select response pairs and then generate corresponding negative images. The collected data are used to update  $\pi_t$ . The filtering strategy is detailed in Section 2.2.

## 2.1 OVERVIEW

As illustrated in Figure 2, our OViP framework is designed to dynamically construct real-time preference pairs during training, by collecting in-distribution success and failure responses along with their corresponding original and synthesized images. These preference pairs are then integrated into the next training iteration for direct preference optimization on both image and response sides, providing a continuous feedback loop that refines the model’s visual grounding and improves its ability to distinguish high-quality outputs from suboptimal ones.

Specifically, given an input image  $\mathcal{I}^+$ , an instruction  $\mathcal{Q}$ , and a reference response  $\mathcal{A}^*$ , OViP first samples multiple candidate responses using the target model  $\pi$ . These responses are then filtered and selected to form positive and negative pairs  $(\mathcal{A}^+, \mathcal{A}^-)$ . Based on the semantic discrepancies between the response pairs, contrastive images  $\mathcal{I}^-$  are further synthesized to describe the negative responses. Finally, both image-level and response-level contrastive losses are applied to update the target model  $\pi$ . A detailed workflow of the OViP algorithm is provided in Table 4.

## 2.2 IN-DISTRIBUTION PREFERENCE DATA CONSTRUCTION

We adopt training-time inference to dynamically construct richer preference pairs reflecting in-distribution failures concurrently with the training process, expanding limited and static offline datasets. Specifically, our method involves three integral stages: (1) real-time generation of candidate outputs given visual inputs and instructions, (2) quality-aware sampling of informative preference pairs, and (3) inverse construction of input data conditioned directly on these sampled outputs. To ensure training stability, we implement dynamic sampling techniques and an experience buffer.

**Real-time Generation of Output Data** At each training step  $s$ , given a visual input  $\mathcal{I}^+$  and its corresponding textual instruction  $\mathcal{Q}$ , our model  $\pi_s$  generates  $k = 16$  candidate responses  $\mathcal{A}^i$  ( $i = 1, 2, \dots, k$ ) through stochastic sampling. Each generated response is then individually evaluated by an LLM-based reward function (denoted as  $G_r$ ), which assigns a numerical reward score to each response, reflecting its alignment with the ground-truth answer  $\mathcal{A}^*$ .

$$\mathcal{A}^i \sim \pi_s (\cdot | \mathcal{I}^+, \mathcal{Q}) ; \quad r^i = G_r (\mathcal{A}^i, \mathcal{A}^*) \quad (1)$$

**Contrasting Response Pair Sampling** To effectively learn from preference data, it is crucial to construct pairs with sufficient contrast in quality (Yu et al., 2025). We dynamically construct preference pairs by selecting response pairs within each batch that display significant score dispari-

ties. Specifically, for each set of candidate responses  $\{\mathcal{A}^i\}_{i=1}^k$  with corresponding rewards  $\{r^i\}_{i=1}^k$ , we compute the standard deviation  $\sigma_r$  of the reward scores and select pairs  $(\mathcal{A}^+, \mathcal{A}^-)$  that satisfy  $|r^+ - r^-| > \max(\delta, 2\sigma_r)$  where  $\delta$  is a fixed lower-bound margin. This criterion ensures that only response pairs exhibiting substantial contrast in reward scores are selected, effectively emphasizing informative differences between success and failure responses. Additionally, we enforce quality constraints by requiring that the accepted positive responses meet a predefined quality criterion (i.e.,  $r^+ > \tau_{\text{pos}}$ ), while rejected negative responses fall below a specified threshold (i.e.,  $r^- < \tau_{\text{neg}}$ ). In cases where all candidate responses collectively perform poorly, we leverage offline ground-truth answers  $\mathcal{A}^*$  as positive responses to guide the model learning effectively, a practice reminiscent of the mixed-policy approach in Yan et al. (2025).

$$\mathcal{D}_{\text{pair}} = \{(\mathcal{Q}, \mathcal{I}^+, \mathcal{A}^+, \mathcal{A}^-) \mid \mathcal{A}^+, \mathcal{A}^- \in \{\mathcal{A}^i\}_{i=1}^k, |r^+ - r^-| > \max(\delta, 2\sigma_r), r^+ > \tau_{\text{pos}}, r^- < \tau_{\text{neg}}\} \quad (2)$$

**Inverse Negative Image Synthesis** After obtaining response pairs  $(\mathcal{Q}, \mathcal{I}^+, \mathcal{A}^+, \mathcal{A}^-) \in \mathcal{D}_{\text{pair}}$ , we synthesize negative images corresponding to negative responses while taking input images as positive. Specifically, we utilize an external LLM (denoted as  $G_{\text{diff}}$ ) to identify a set of semantic differences between the positive and negative responses, including entities, attributes, and spatial relations, and then generate a textual description  $\mathcal{T}^- = G_{\text{diff}}(\mathcal{Q}, \mathcal{A}^+, \mathcal{A}^-)$  that encapsulates the semantic content of the negative response  $\mathcal{A}^-$ . Subsequently, a diffusion-based image generation model (denoted as  $\text{Diff}$ ) synthesizes a hard negative image as follows:

$$\mathcal{I}^- = \text{Diff}(\mathcal{T}^-) \quad (3)$$

This inverse generation process, in which the image is conditioned on the textual output, ensures that the synthesized image captures hallucinated or incorrect content, providing more targeted supervision for hallucination mitigation. Moreover, as the generation is explicitly driven by response-level discrepancies, the resulting negative images exhibit higher semantic relevance and visual specificity.

**Dynamic Inference and Experience Buffer** To stabilize batch-wise training while retaining the flexibility of online sampling, we maintain an experience buffer  $\mathcal{B}$  that stores dynamically constructed contrastive training samples. At each training step, the current model  $\pi_s$  performs inference and response sampling, producing contrastive samples that are continuously added to  $\mathcal{B}$ . This sampling process persists until the accumulated samples reach the predefined batch size  $N$ . Once  $|\mathcal{B}| \geq N$ , a batch of  $N$  samples is retrieved from  $\mathcal{B}$  for loss computation and gradient updates. The remaining samples in the buffer are preserved for subsequent iterations, ensuring the training process to proceed smoothly even under variable sampling yields.

### 2.3 IMAGE- AND RESPONSE-SIDE PREFERENCE OPTIMIZATION

To effectively align both textual and visual modalities during training, we formulate a unified optimization framework that simultaneously considers response-level and image-level preference signals. The overall optimization objective consists of two complementary components. The first is the text DPO loss (Rafailov et al., 2023), which guides the model to learn response-level preferences conditioned on the input image and instruction:

$$\mathcal{L}_{\text{Text}}(\mathcal{A}^+, \mathcal{A}^-; \mathcal{I}^+, \mathcal{Q}) = -\log \sigma \left( \beta \cdot \left[ \log \frac{\pi_\theta(\mathcal{A}^+ | \mathcal{I}^+, \mathcal{Q})}{\pi_{\text{ref}}(\mathcal{A}^+ | \mathcal{I}^+, \mathcal{Q})} - \log \frac{\pi_\theta(\mathcal{A}^- | \mathcal{I}^+, \mathcal{Q})}{\pi_{\text{ref}}(\mathcal{A}^- | \mathcal{I}^+, \mathcal{Q})} \right] \right) \quad (4)$$

In addition to response-level alignment, we incorporate a contrastive objective focused on the visual input. By keeping the query and response fixed, the model is required to learn preferences solely from differences in the visual input. On top of this, to further ensure that the model’s output maintains a reasonable and smooth probability distribution, we introduce the image-free term  $\pi_\theta(\mathcal{A} | \mathcal{Q})$  and implement the image-side loss as in Wu et al. (2025):

$$\begin{aligned} \mathcal{L}_{\text{Image}}(\mathcal{I}^+, \mathcal{I}^-; \mathcal{Q}, \mathcal{A}^+) = & -\log \sigma \left( \beta_1 \cdot \left[ \log \frac{\pi_\theta(\mathcal{A}^+ | \mathcal{I}^+, \mathcal{Q})}{\pi_{\text{ref}}(\mathcal{A}^+ | \mathcal{I}^+, \mathcal{Q})} - \log \frac{\pi_\theta(\mathcal{A}^+ | \mathcal{Q})}{\pi_{\text{ref}}(\mathcal{A}^+ | \mathcal{Q})} \right] \right. \\ & \left. + \beta_2 \cdot \left[ \log \frac{\pi_\theta(\mathcal{A}^+ | \mathcal{Q})}{\pi_{\text{ref}}(\mathcal{A}^+ | \mathcal{Q})} - \log \frac{\pi_\theta(\mathcal{A}^+ | \mathcal{I}^-, \mathcal{Q})}{\pi_{\text{ref}}(\mathcal{A}^+ | \mathcal{I}^-, \mathcal{Q})} \right] \right) \end{aligned} \quad (5)$$

The overall loss function is then defined as:

$$\mathcal{L}_{\text{OViP}}(\mathcal{Q}, \mathcal{I}^+, \mathcal{I}^-, \mathcal{A}^+, \mathcal{A}^-) = \mathcal{L}_{\text{Text}}(\mathcal{A}^+, \mathcal{A}^-; \mathcal{I}, \mathcal{Q}) + \mathcal{L}_{\text{Image}}(\mathcal{I}^+, \mathcal{I}^-; \mathcal{Q}, \mathcal{A}^+) \quad (6)$$

---

### 3 EXPERIMENT

#### 3.1 EXPERIMENTAL SETUP

**Implementation Details** We conduct our experiments on LLaVA-1.5-7B-hf and LLaVA-1.5-13B-hf (Liu et al., 2024b), with CLIP ViT-L-336px as the visual encoder and Vicuna-7b/13b as the backbone respectively. The training dataset, sourced from Yang et al. (2025), consists of 8,730 samples and 4,013 distinct image–query combinations, including image description, question answering, and some yes/no questions. We use LoRA (Hu et al., 2022) with a rank of 256 and alpha of 512. Other settings are listed in Appendix B.2

**Baselines** We compare OViP with SFT, DPO (Rafailov et al., 2023), mDPO (Wang et al., 2024a) and GRPO (Shao et al., 2024). As the original versions of SFT, DPO and mDPO are offline methods, we additionally implement iterative DPO and GRPO to facilitate a more comprehensive comparison. Furthermore, we evaluate several prior works with publicly available model weights, including HA-DPO (Zhao et al., 2023), HALVA (Sarkar et al., 2024), RLAIF-V (Yu et al., 2024b) and OPA-DPO (Yang et al., 2025). Among them, our OViP and OPA-DPO use the same original training data, which is a subset of the dataset used by RLAIF-V.

#### 3.2 EVALUATION METRICS

We conduct evaluations on five **hallucination-related** and four **general capability** benchmarks to assess hallucination mitigation and overall capability degradation.

**Hallucination-Related Evaluation.** We evaluate hallucination in LVLM outputs using MMHal-Bench (MMHal) (Sun et al., 2024), AMBER generative ( $AMB_{gen}$ ) (Wang et al., 2023), Object HalBench (ObjectHal) (Rohrbach et al., 2018), Llava-Bench-in-the-Wild (LV) (Liu et al., 2023), and AMBER discriminative ( $AMB_{dis}$ ) (Wang et al., 2023). Detailed descriptions of the datasets, evaluation procedures, and metrics are provided in Appendix A.2

Prior work has primarily focused on assessing the precision of model outputs, i.e., whether the generated content contains explicit hallucinations. However, this perspective often overlooks the *completeness* of the output: a model may omit relevant entities (especially in image description tasks), leading to what we term *implicit hallucinations*. *We argue that both explicit and implicit hallucinations are critical for a faithful evaluation of model reliability.* Building on this perspective and the observation of failure cases where existing benchmarks can be hacked, we **refine the evaluation protocols and introduce an F1 score for  $AMB_{gen}$  and ObjectHal to better capture the extent of hallucination in generated responses**. Illustrative failure cases of prior evaluation strategies are presented in Appendix A.3.

To aggregate performance across five benchmarks, we introduce the **Hallucination Reduction Index (HRI)** as a unified measure of overall improvement. HRI is computed by summing the normalized improvements from each benchmark to obtain the overall relative gain. The detailed calculation of HRI and the discussion of its fairness are provided in Appendix A.1.

**General Capability Evaluation** To assess the trade-off between hallucination mitigation and general visual capability, we evaluate the trained models on general benchmarks, including Real-worldQA (xAI, 2024), TextVQA (Singh et al., 2019), CVBench (Tong et al., 2024), MMStar (Chen et al., 2024b). We aggregate the results across these benchmarks and compute the **Accuracy Difference**, serving as a unified metric to quantify overall performance variation after training.

#### 3.3 MAIN RESULTS

Table 1 presents results for OViP and other methods across multiple benchmarks on various LVLM backbones. **OViP consistently achieves significant improvements across most primary metrics while effectively preserving the model’s general visual capabilities** (achieving +0.88 with one epoch for General  $Acc_{Dif}$  and a slight drop of -1.01 for 2 epochs), whereas most other methods that exhibit varying degrees of degradation in general benchmarks. Moreover, OViP further improves

Table 1: **Main Results for OViP and other methods across different benchmarks.** The five shaded metrics highlight the primary balanced and overall results for each benchmark. **HRI** (Hallucination Reduction Index) is the average improvement across five benchmarks.  $Acc_{dif}$  is the total accuracy changes across TextVQA(Singh et al., 2019), RealworldQA(xAI, 2024), MMStar(Chen et al., 2024b) and CVBench(Tong et al., 2024). GPT4-V( $\dagger$ )’s results are cited from Xiao et al. (2025),Wang et al. (2023),Duan et al. (2024) for reference.  $\ddagger$  indicates the use of original evaluation strategy.  $*$  denotes methods with publicly released model weights trained on their own datasets, which we direct evaluate without re-training.  $\ddagger$  signifies methods trained on datasets that are the same as or larger than ours. “2-ep” specifies results obtained after two epochs of training. We separate offline methods from non-offline methods for clearer comparison.

	Chair $\downarrow$	AMB <sub>gen</sub> Cover $\uparrow$	MMHal Score $\uparrow$	ObjectHal		LV Score $\uparrow$	AMB <sub>dis</sub> F1 $\uparrow$	<b>HRI</b>	General Acc <sub>Dif</sub>
				Chair $_r \downarrow$	F1 $\uparrow$				
LLaVA-1.5-7B	GPT4-V $\dagger$	4.6	67.1	78.8	3.49 $\ddagger$	13.6	-	95.3	87.4
	Baseline	7.1	50.0	65.01	1.90	51.38	72.40	57.20	85.5
	HA-DPO*	5.6	49.4	64.86	1.95	37.15	73.81	57.30	85.4
	HALVA*	5.7	52.9	<b>67.78</b>	2.12	43.40	<b>76.01</b>	58.60	86.5
	RLAIF-V* $\ddagger$	3.1	49.8	65.79	2.54	9.35	69.78	58.90	86.4
	OPA-DPO* $\ddagger$	2.4	45.2	<b>61.79</b>	<b>2.78</b>	6.37	63.26	<b>64.80</b>	86.7
	SFT	3.5	50.6	66.39	2.52	20.60	70.30	52.20	86.1
	DPO	3.7	48.9	64.86	2.35	26.60	71.95	56.70	86.8
	mDPO	3.4	48.6	64.67	<b>2.55</b>	25.45	<b>73.92</b>	55.80	86.1
	DPO <sub>iterative</sub>	3.9	48.7	64.64	2.32	27.11	72.33	56.40	86.5
LLaVA-1.5-13B	GRPO <sub>2ep</sub>	4.8	51.2	66.59	2.45	34.98	73.83	58.70	86.8
	<b>OViP</b>	4.0	51.1	<b>66.70</b>	2.52	33.22	73.50	<b>63.10</b>	<b>87.3</b>
	<b>OViP</b> <sub>2ep</sub>	4.0	51.6	<b>67.12</b>	<b>2.65</b>	29.54	<b>74.18</b>	<b>60.90</b>	<b>87.4</b>
	Baseline	6.5	51.0	65.99	2.24	46.18	76.73	62.60	89.1
	HALVA*	6.0	52.2	67.12	2.45	35.07	<b>77.75</b>	61.70	90.0
	OPA-DPO* $\ddagger$	2.8	47.8	64.08	<b>2.88</b>	5.88	64.46	64.70	89.3
	SFT	4.5	50.0	65.64	2.38	31.21	75.81	64.00	89.9
	DPO	3.6	50.6	66.37	2.53	25.00	75.00	65.30	89.6
	mDPO	3.9	50.1	65.86	2.51	21.79	75.35	64.50	89.5
	GRPO <sub>2ep</sub>	3.8	52.4	67.84	2.38	23.76	75.55	<b>66.70</b>	<b>90.4</b>
	<b>OViP</b>	4.4	53.1	<b>68.28</b>	<b>2.58</b>	36.30	76.52	64.60	89.7
	<b>OViP</b> <sub>2ep</sub>	3.6	53.7	<b>68.98</b>	2.57	28.62	<b>76.75</b>	<b>67.90</b>	<b>90.2</b>
								<b>8.02</b>	<b>+2.02</b>

with an additional training epoch. Notably, even with one epoch, OViP surpasses HALVA and 2-epoch GRPO, both of which utilize twice as much training data, but still yield lower HRI and suffer from general ability degradation.

A critical phenomenon often overlooked in previous work (Xie et al., 2024; Yang et al., 2025; Fu et al., 2025; Xiao et al., 2025; Wang et al., 2024a; Yu et al., 2024a;b) is that **offline methods generally impair models’ general capability while also introducing implicit hallucinations** (as discussed in subsection 3.2). This issue is particularly evident in OPADPO, where Chair score on  $AMB_{gen}$  drops to 2.4, and Cover metric decreases from the initial 50.0 to 45.2, far below other methods. An illustrative example of such omission is in Figure 9 in Appendix. Moreover, excessive training further exacerbates this problem: as shown in Table 1, several DPO-like methods (HA-DPO, HALVA, RLAIF-V, OPA-DPO) trained for more than two epochs suffer from much larger declines in general capability compared to DPO and mDPO trained for only one epoch. At the same time, except for HALVA, their HRI scores are also lower than those of DPO and mDPO, which mainly influenced by the low F1 scores on  $AMB_{gen}$  and ObjectHal. *With these possible signs of overfitting, we suggest that some improvements reported in prior work may be overestimated.*

### 3.4 ABLATION STUDY

**The Impact of Loss functions.** We evaluated various combinations of loss functions for on-line preference learning in hallucination mitigation to derive the final formulation in Equation 6. Our ablation study examines the effectiveness of different training objectives, including text-side ( $\mathcal{L}_{Text}$ ), image-side and auxiliary losses. Specifically for image-side losses, we examine our image loss  $\mathcal{L}_{Image}$  alongside two variants  $\mathcal{L}_{Image}^{base}$  and  $\mathcal{L}_{Image-Sym}$ . For auxiliary loss, we compare the anchor loss proposed by Wang et al. (2024a) and the bidirectional anchor loss, which enforce the

probability of positive response to increase and the negative one to decrease. Detailed formulations are provided in Appendix B.1.

Table 2: Results of different loss functions.  
 $\mathcal{L}_{\text{OViP}} = \mathcal{L}_{\text{Text}} + \mathcal{L}_{\text{Image}}$ .

Loss Functions	HRI	
	From Scratch	Iterative
$\mathcal{L}_{\text{OViP}}$	<b>4.32</b>	<b>7.94</b>
– $\mathcal{L}_{\text{Text}}$	4.23	7.71
– $\mathcal{L}_{\text{Image}}$	-2.29	4.56
$\mathcal{L}_{\text{Text}} + \mathcal{L}_{\text{Image}}^{\text{base}}$	4.08	7.50
$\mathcal{L}_{\text{Image-Sym}}$	-0.32	6.57

Table 3: Results of offline and online training strategy with DPO and OViP. Cover measures the informativeness of the model from  $\text{AMB}_{\text{gen}}$ . Cover score of the original model is 50.

Method	Cover	HRI	General Acc <sub>Dif</sub>
OViP	online	<b>51.1</b>	<b>9.36</b>
	offline	49.9	4.32
DPO	online	<b>50.0</b>	<b>1.71</b>
	offline	48.3	-2.29
			<b>-1.38</b>

We conduct experiments under two training regimes: (1) training from scratch, and (2) iterative training initialized with a DPO-pretrained model using the existing dataset, to ablate these losses on top of different initialized models with varying capabilities. We observe that models trained with different losses do not suffer from a notable drop in general ability ( $\text{General Acc}_{\text{Dif}} > -1.5$ ). Therefore, in Table 2 we only report the HRI results, which show that the full OViP loss consistently outperforms all variants under both training regimes. Moreover, the form of the image loss greatly affects the results, with the loss in Equation 5 achieving the best performance.

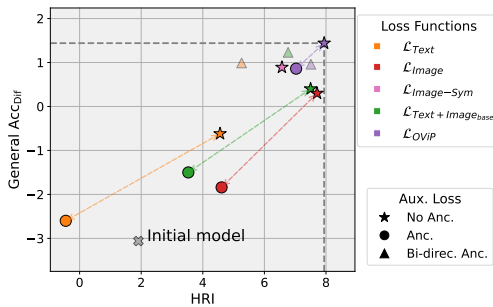


Figure 3: Effect of applying auxiliary loss to different loss functions.

Under the same iterative training regime, we further analyze the effect of auxiliary losses based on the DPO-initialized model and its sampled responses, as illustrated in Figure 3. Contrary to the findings in mDPO (Wang et al., 2024a), we find that **incorporating anchor loss consistently reduces general capability and increases hallucinations across all loss combinations**. Moreover, while applying bi-directional anchor loss slightly improves general capabilities, it does not necessarily enhance hallucination mitigation. Therefore, OViP loss without anchor loss is the most effective training objective for both reducing hallucination and maintaining general ability.

**Online v.s. Offline.** Table 3 demonstrates that online training consistently outperforms its offline counterpart in HRI by at least 4 points within just one epoch (and continues to improve with further training, while offline training suffers from overfitting). Another notable observation is that *online training also improves the informativeness of model outputs*. Even when trained with DPO, the Cover score remains 50. In contrast, previous studies (Yu et al., 2024b; Yang et al., 2025; Fu et al., 2025) using the similar dataset typically exhibit a drop in this aspect. Additionally, the improvement for online training over offline training is almost across every individual benchmark and each corresponding metric, online training yields more stable and superior performance. Detailed results are provided in Appendix B.3.

## 4 FURTHER STUDY

### 4.1 TRAINING EFFICIENCY

Although OViP requires constructing negative images, which needs additional GPU resources for deploying diffusion models and incurs extra time overhead, we show that OViP still has clear advantages in overall training efficiency. In Figure 4, we compare different online methods by plotting their HRI and general capability against expected GPU hours. (A detailed analysis of training cost and efficiency is provided in Appendix D) *The results show that despite slower per-iteration*

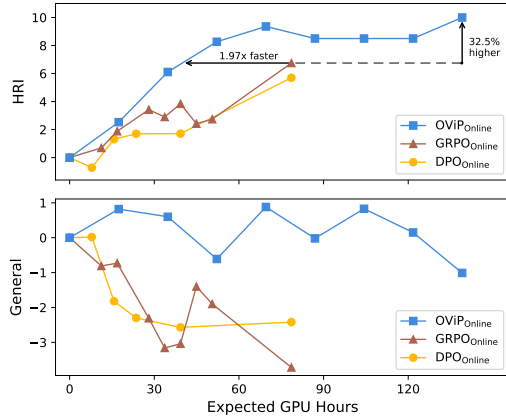


Figure 4: **Performance comparison among online training methods up to 2 epochs.** The X-axis shows the expected training time multiplied by the number of GPUs used. OViP outperforms GRPO with  $1.97\times$  higher training efficiency.

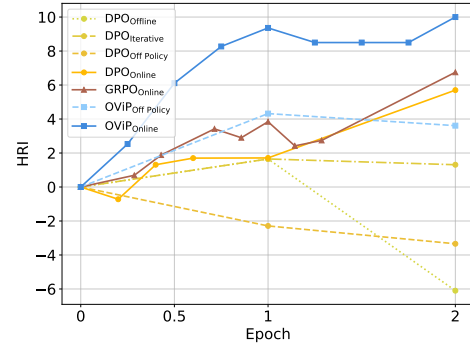


Figure 5: **Results under different training strategies.** Offline denotes training with the existing dataset; Off Policy refers to training with sampled data; and Iterative indicates that the dataset for the second epoch is generated by sampling from the offline-trained model after the first epoch.

speed, OViP achieves approximately  $1.97\times$  higher training efficiency than GRPO. OViP requires only about half the computation of GRPO to achieve comparable performance, while Online DPO performs slightly worse than GRPO. As for offline approaches, although their data construction and training require a similar amount of computation, their performance consistently falls short of their online counterparts; hence, our efficiency comparison focuses on online methods.

#### 4.2 TRAINING DYNAMICS

Figure 5 illustrates how HRI evolves during training under different strategies, which allows us to investigate the dynamics of hallucination throughout training.

**Need for Visual and Online Signals** For hallucination mitigation in LLMs, *adding visual supervision signals proves crucial*: offline OViP surpasses GRPO and all DPO variants with one epoch. Building on this, *online methods offer further advantages, which not only make each optimization step more effective in reducing hallucinations, but also exhibit better scalability*, with overfitting arising significantly later compared to non-online approaches, whose performance starts to drop after training for one epoch. We conjecture that this superiority stems from the model-specific nature of hallucinations, which requires supervision to precisely target the current model’s errors.

**Early Training Stagnation** Both Online DPO and Off-Policy DPO exhibit an initial drop in performance, while GRPO and OViP show relatively slow improvement during the early stages of training. We attribute this phenomenon to the model’s initially skewed output distribution. Early training primarily increases the diversity of model outputs, which does not immediately translate into performance gains but expands the search space for subsequent learning. A detailed discussion is provided in Appendix B.4.

#### 4.3 WHAT DO WE ACTUALLY OPTIMIZE DURING TRAINING?

We investigate how training affects the distribution of response quality, as shown in Figure 6. The results indicate that performance gains come from both reducing hallucinated outputs and increasing high-quality ones. After training, responses with scores below 6 become less likely, while those above 6 occur more frequently.

*Online training yields additional benefits over offline DPO. It further lowers the probability of severely hallucinated responses (score < 3) and raises the probability of very high-quality ones (score > 9), whereas offline DPO hardly changes the distribution at these extremes. Adding visual*

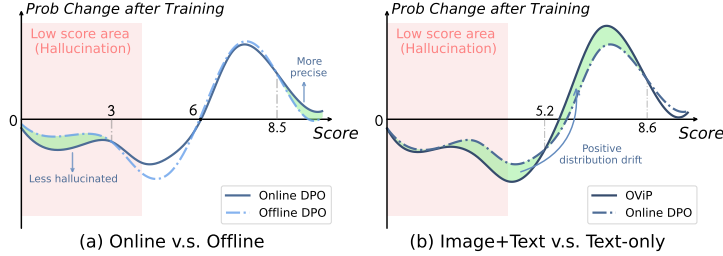


Figure 6: Change in probability mass for the responses with corresponding score after training. “Low score” refers to scores less than 4. We smooth the discrete probability changes over 11 score bins (0-10) into a continuous curve. “Change  $> 0$ ” represents the probability increases after training.

*supervision signals shifts the overall distribution in a positive direction*, though it makes little extra difference to the probabilities at the lowest and highest scores. These observations suggest that the benefits of online training and those of visual supervision are orthogonal, thereby explaining OViP’s stronger improvements achieved.

## 5 RELATED WORK

### 5.1 LVLM HALLUCINATION

Works of synthetic data construction for mitigating hallucination in LVLMs can be broadly categorized into image-related synthesis and text-only synthesis. On the image side, several approaches leverage entity extraction and masking to perform targeted image editing, generating visually similar but semantically distinct counterfactuals (Xie et al., 2024; Lu et al., 2025). In contrast, Hallusion-Bench (Guan et al., 2024) adopts a manual approach, carefully crafting counterfactual images to probe specific failure modes. Other works take a generative perspective: SynthVLM (Liu et al., 2024c) and SynthEmbedding (Sharifzadeh et al., 2024) utilize off-the-shelf models to synthesize new images or directly generate image embeddings for hallucination-aware training. Meanwhile, text-side data augmentation can also be used in LVLM training. VoCoT (Li et al., 2024) introduces new prompting patterns and response types to generate hallucination-prone QA data at scale. Other works such as Zhou et al. (2024a), Sarkar et al. (2024), Amirloo et al. (2024) introduce noise through perturbation, masking, or controlled corruption to simulate erroneous responses. More recent approaches (Xiao et al., 2025; Yu et al., 2024a) aim to detect and correct hallucinated content at varying levels of granularity, from token-level edits to full-sequence rewrites.

These efforts significantly improve the diversity and coverage of supervision signals available for training hallucination-robust VLMs.

### 5.2 ALLOCATING MORE COMPUTATION ON TRAINING SAMPLE CONSTRUCTION

Recent research has increasingly adopted the paradigm of allocating additional computation during training to get better training samples. Several studies utilize reinforcement learning with human or AI-generated feedback to guide VLM outputs. RLHF-V (Yu et al., 2024a) leverages fine-grained human annotations to correct hallucinated content, while RLAIF-V (Yu et al., 2024b) replaces human labels with feedback from ensembles of open-source models, significantly reducing annotation overhead. Similarly, OPA-DPO (Yang et al., 2025) employs an on-policy editing step prior to DPO, aligning training samples closely with model predictions to enhance data efficiency. CLIP-based methods dynamically filter self-generated samples for high-quality training pairs (Ouali et al., 2024; Zhou et al., 2024b). Other methods integrate auxiliary reward models or evaluators during training, providing continuous and adaptive feedback loops (Sun et al., 2024; Yan et al., 2024). Additionally, recent approaches incorporate reasoning or editing mechanisms directly into training, using iterative self-feedback or generative data augmentation techniques to dynamically refine model outputs (Zhao et al., 2023; Kim et al., 2024). These strategies improve model alignment and factuality by enriching the quality and relevance of supervision signals during training.

---

## 6 CONCLUSION

In this work, we propose the Online Vision-language Preference Learning (OViP) framework to efficiently address the hallucination problem in LVLMs. By integrating online preference learning with image-aware training, OViP enables real-time construction of high-quality contrastive data during training. Furthermore, to better assess the trade-offs between hallucination reduction and overall performance, we refine and extend existing evaluation protocols. Experimental results demonstrate that OViP significantly outperforms prior offline/online training approaches, achieving substantial hallucination reduction while preserving general vision-language capabilities, which many existing offline methods fail to preserve. Our investigation into training dynamics also sheds light on the underlying mechanisms behind OViP’s effectiveness.

---

## ETHICS STATEMENT

This work focuses on improving the factual reliability of vision-language models by reducing hallucination. While it does not directly engage with societal applications, it contributes to the broader goal of building more trustworthy and robust AI systems. Although the method itself does not pose obvious risks, we note that even improved generation quality does not eliminate the possibility of misuse, such as producing misleading content. Responsible deployment and proper safeguards remain necessary when integrating such models into real-world applications.

## REPRODUCIBILITY STATEMENT

We provide detailed descriptions of the training and evaluation setups in Appendix A and Appendix B. In addition, we include anonymized training and evaluation code, instructions for running the experiments, and information on accessing the relevant datasets in the supplementary materials.

## REFERENCES

Jean-Baptiste Alayrac, Jeff Donahue, Pauline Luc, Antoine Miech, Iain Barr, Yana Hasson, Karel Lenc, Arthur Mensch, Katherine Millican, Malcolm Reynolds, et al. Flamingo: a visual language model for few-shot learning. *Advances in neural information processing systems*, 35:23716–23736, 2022.

Elmira Amirloo, Jean-Philippe Fauconnier, Christoph Roesmann, Christian Kerl, Rinu Boney, Yusu Qian, Zirui Wang, Afshin Dehghan, Yinfei Yang, Zhe Gan, et al. Understanding alignment in multimodal llms: A comprehensive study. *arXiv preprint arXiv:2407.02477*, 2024.

Jinze Bai, Shuai Bai, Yunfei Chu, Zeyu Cui, Kai Dang, Xiaodong Deng, Yang Fan, Wenbin Ge, Yu Han, Fei Huang, et al. Qwen technical report. *arXiv preprint arXiv:2309.16609*, 2023.

Zechen Bai, Pichao Wang, Tianjun Xiao, Tong He, Zongbo Han, Zheng Zhang, and Mike Zheng Shou. Hallucination of multimodal large language models: A survey. *arXiv preprint arXiv:2404.18930*, 2024.

Jun Chen, Deyao Zhu, Xiaoqian Shen, Xiang Li, Zechun Liu, Pengchuan Zhang, Raghuraman Krishnamoorthi, Vikas Chandra, Yunyang Xiong, and Mohamed Elhoseiny. Minigpt-v2: large language model as a unified interface for vision-language multi-task learning. *arXiv preprint arXiv:2310.09478*, 2023.

Lin Chen, Jinsong Li, Xiaoyi Dong, Pan Zhang, Conghui He, Jiaqi Wang, Feng Zhao, and Dahua Lin. Sharegpt4v: Improving large multi-modal models with better captions. In *European Conference on Computer Vision*, pp. 370–387. Springer, 2024a.

Lin Chen, Jinsong Li, Xiaoyi Dong, Pan Zhang, Yuhang Zang, Zehui Chen, Haodong Duan, Jiaqi Wang, Yu Qiao, Dahua Lin, et al. Are we on the right way for evaluating large vision-language models? *arXiv preprint arXiv:2403.20330*, 2024b.

Wenliang Dai, Junnan Li, Dongxu Li, Anthony Meng Huat Tiong, Junqi Zhao, Weisheng Wang, Boyang Li, Pascale Fung, and Steven Hoi. Instructblip: Towards general-purpose vision-language models with instruction tuning, 2023. URL <https://arxiv.org/abs/2305.06500>.

Haodong Duan, Junming Yang, Yuxuan Qiao, Xinyu Fang, Lin Chen, Yuan Liu, Xiaoyi Dong, Yuhang Zang, Pan Zhang, Jiaqi Wang, et al. Vlmevalkit: An open-source toolkit for evaluating large multi-modality models. In *Proceedings of the 32nd ACM International Conference on Multimedia*, pp. 11198–11201, 2024.

Jinlan Fu, Shenzhen Huangfu, Hao Fei, Xiaoyu Shen, Bryan Hooi, Xipeng Qiu, and See-Kiong Ng. Chip: Cross-modal hierarchical direct preference optimization for multimodal llms, 2025. URL <https://arxiv.org/abs/2501.16629>.

---

Tianrui Guan, Fuxiao Liu, Xiyang Wu, Ruiqi Xian, Zongxia Li, Xiaoyu Liu, Xijun Wang, Lichang Chen, Furong Huang, Yaser Yacoob, et al. Hallusionbench: an advanced diagnostic suite for entangled language hallucination and visual illusion in large vision-language models. In *Proceedings of the IEEE/CVF Conference on Computer Vision and Pattern Recognition*, pp. 14375–14385, 2024.

Shangmin Guo, Biao Zhang, Tianlin Liu, Tianqi Liu, Misha Khalman, Felipe Llinares, Alexandre Rame, Thomas Mesnard, Yao Zhao, Bilal Piot, et al. Direct language model alignment from online ai feedback. *arXiv preprint arXiv:2402.04792*, 2024.

Edward J Hu, Yelong Shen, Phillip Wallis, Zeyuan Allen-Zhu, Yuanzhi Li, Shean Wang, Lu Wang, Weizhu Chen, et al. Lora: Low-rank adaptation of large language models. *ICLR*, 1(2):3, 2022.

Minchan Kim, Minyeong Kim, Junik Bae, Suhwan Choi, Sungkyung Kim, and Buru Chang. Exploiting semantic reconstruction to mitigate hallucinations in vision-language models. In *European Conference on Computer Vision*, pp. 236–252. Springer, 2024.

Junnan Li, Dongxu Li, Silvio Savarese, and Steven Hoi. Blip-2: Bootstrapping language-image pre-training with frozen image encoders and large language models. In *International conference on machine learning*, pp. 19730–19742. PMLR, 2023a.

Yifan Li, Yifan Du, Kun Zhou, Jinpeng Wang, Wayne Xin Zhao, and Ji-Rong Wen. Evaluating object hallucination in large vision-language models. *arXiv preprint arXiv:2305.10355*, 2023b.

Zejun Li, Ruipu Luo, Jiwen Zhang, Minghui Qiu, Xuanjing Huang, and Zhongyu Wei. Vocot: Unleashing visually grounded multi-step reasoning in large multi-modal models. *arXiv preprint arXiv:2405.16919*, 2024.

Hanchao Liu, Wenyuan Xue, Yifei Chen, Dapeng Chen, Xiutian Zhao, Ke Wang, Liping Hou, Rongjun Li, and Wei Peng. A survey on hallucination in large vision-language models. *arXiv preprint arXiv:2402.00253*, 2024a.

Haotian Liu, Chunyuan Li, Qingyang Wu, and Yong Jae Lee. Visual instruction tuning. *Advances in neural information processing systems*, 36:34892–34916, 2023.

Haotian Liu, Chunyuan Li, Yuheng Li, and Yong Jae Lee. Improved baselines with visual instruction tuning. In *Proceedings of the IEEE/CVF Conference on Computer Vision and Pattern Recognition*, pp. 26296–26306, 2024b.

Zheng Liu, Hao Liang, Xijie Huang, Wentao Xiong, Qinhan Yu, Linzhuang Sun, Chong Chen, Conghui He, Bin Cui, and Wentao Zhang. Synthvilm: High-efficiency and high-quality synthetic data for vision language models. *arXiv preprint arXiv:2407.20756*, 2024c.

Jinda Lu, Jinghan Li, Yuan Gao, Junkang Wu, Jiancan Wu, Xiang Wang, and Xiangnan He. Adavip: Aligning multi-modal llms via adaptive vision-enhanced preference optimization. *arXiv preprint arXiv:2504.15619*, 2025.

Yassine Ouali, Adrian Bulat, Brais Martinez, and Georgios Tzimiropoulos. Clip-dpo: Vision-language models as a source of preference for fixing hallucinations in l1lms. In *European Conference on Computer Vision*, pp. 395–413. Springer, 2024.

Rafael Rafailov, Archit Sharma, Eric Mitchell, Christopher D Manning, Stefano Ermon, and Chelsea Finn. Direct preference optimization: Your language model is secretly a reward model. In A. Oh, T. Naumann, A. Globerson, K. Saenko, M. Hardt, and S. Levine (eds.), *Advances in Neural Information Processing Systems*, volume 36, pp. 53728–53741. Curran Associates, Inc., 2023. URL [https://proceedings.neurips.cc/paper\\_files/paper/2023/file/a85b405ed65c6477a4fe8302b5e06ce7-Paper-Conference.pdf](https://proceedings.neurips.cc/paper_files/paper/2023/file/a85b405ed65c6477a4fe8302b5e06ce7-Paper-Conference.pdf).

Anna Rohrbach, Lisa Anne Hendricks, Kaylee Burns, Trevor Darrell, and Kate Saenko. Object hallucination in image captioning. In *Proceedings of the 2018 Conference on Empirical Methods in Natural Language Processing*, pp. 4035–4045, 2018.

---

Pritam Sarkar, Sayna Ebrahimi, Ali Etemad, Ahmad Beirami, Sercan Ö Arik, and Tomas Pfister. Data-augmented phrase-level alignment for mitigating object hallucination. *arXiv preprint arXiv:2405.18654*, 2024.

Zhihong Shao, Peiyi Wang, Qihao Zhu, Runxin Xu, Junxiao Song, Xiao Bi, Haowei Zhang, Mingchuan Zhang, YK Li, Y Wu, et al. Deepseekmath: Pushing the limits of mathematical reasoning in open language models. *arXiv preprint arXiv:2402.03300*, 2024.

Sahand Sharifzadeh, Christos Kaplanis, Shreya Pathak, Dharshan Kumaran, Anastasija Ilic, Jovana Mitrovic, Charles Blundell, and Andrea Banino. Synth<sup>2</sup>: Boosting visual-language models with synthetic captions and image embeddings. *arXiv preprint arXiv:2403.07750*, 2024.

Amanpreet Singh, Vivek Natarajan, Meet Shah, Yu Jiang, Xinlei Chen, Dhruv Batra, Devi Parikh, and Marcus Rohrbach. Towards vqa models that can read. In *Proceedings of the IEEE/CVF conference on computer vision and pattern recognition*, pp. 8317–8326, 2019.

Zhiqing Sun, Sheng Shen, Shengcao Cao, Haotian Liu, Chunyuan Li, Yikang Shen, Chuang Gan, Liangyan Gui, Yu-Xiong Wang, Yiming Yang, et al. Aligning large multimodal models with factually augmented rlhf. In *Findings of the Association for Computational Linguistics ACL 2024*, pp. 13088–13110, 2024.

Shengbang Tong, Ellis Brown, Penghao Wu, Sanghyun Woo, Manoj Middepogu, Sai Charitha Akula, Jihan Yang, Shusheng Yang, Adithya Iyer, Xichen Pan, Austin Wang, Rob Fergus, Yann LeCun, and Saining Xie. Cambrian-1: A fully open, vision-centric exploration of multimodal llms. In A. Globerson, L. Mackey, D. Belgrave, A. Fan, U. Paquet, J. Tomczak, and C. Zhang (eds.), *Advances in Neural Information Processing Systems*, volume 37, pp. 87310–87356. Curran Associates, Inc., 2024. URL [https://proceedings.neurips.cc/paper\\_files/paper/2024/file/9ee3a664ccfeabc0da16ac6f1f1cfe59-Paper-Conference.pdf](https://proceedings.neurips.cc/paper_files/paper/2024/file/9ee3a664ccfeabc0da16ac6f1f1cfe59-Paper-Conference.pdf).

Fei Wang, Wenxuan Zhou, James Y Huang, Nan Xu, Sheng Zhang, Hoifung Poon, and Muhaao Chen. mdpo: Conditional preference optimization for multimodal large language models. In *Proceedings of the 2024 Conference on Empirical Methods in Natural Language Processing*, pp. 8078–8088, 2024a.

Junyang Wang, Yuhang Wang, Guohai Xu, Jing Zhang, Yukai Gu, Haitao Jia, Jiaqi Wang, Haiyang Xu, Ming Yan, Ji Zhang, et al. Amber: An llm-free multi-dimensional benchmark for mllms hallucination evaluation. *arXiv preprint arXiv:2311.07397*, 2023.

Peng Wang, Shuai Bai, Sinan Tan, Shijie Wang, Zhihao Fan, Jinze Bai, Keqin Chen, Xuejing Liu, Jialin Wang, Wenbin Ge, et al. Qwen2-vl: Enhancing vision-language model’s perception of the world at any resolution. *arXiv preprint arXiv:2409.12191*, 2024b.

Shengguang Wu, Fan-Yun Sun, Kaiyue Wen, and Nick Haber. Symmetrical visual contrastive optimization: Aligning vision-language models with minimal contrastive images. *arXiv preprint arXiv:2502.13928*, 2025.

xAI. Grok-1.5 vision preview, April 2024. URL <https://x.ai/blog/grok-1.5v>. Accessed: 2024-12-12.

Wenyi Xiao, Ziwei Huang, Leilei Gan, Wanggui He, Haoyuan Li, Zhelun Yu, Fangxun Shu, Hao Jiang, and Linchao Zhu. Detecting and mitigating hallucination in large vision language models via fine-grained ai feedback. In *Proceedings of the AAAI Conference on Artificial Intelligence*, volume 39, pp. 25543–25551, 2025.

Yuxi Xie, Guanzhen Li, Xiao Xu, and Min-Yen Kan. V-dpo: Mitigating hallucination in large vision language models via vision-guided direct preference optimization. *arXiv preprint arXiv:2411.02712*, 2024.

Jianhao Yan, Yafu Li, Zican Hu, Zhi Wang, Ganqu Cui, Xiaoye Qu, Yu Cheng, and Yue Zhang. Learning to reason under off-policy guidance. *arXiv preprint arXiv:2504.14945*, 2025.

---

Siming Yan, Min Bai, Weifeng Chen, Xiong Zhou, Qixing Huang, and Li Erran Li. Vigor: Improving visual grounding of large vision language models with fine-grained reward modeling. In *European Conference on Computer Vision*, pp. 37–53. Springer, 2024.

Zhihe Yang, Xufang Luo, Dongqi Han, Yunjian Xu, and Dongsheng Li. Mitigating hallucinations in large vision-language models via dpo: On-policy data hold the key. *arXiv preprint arXiv:2501.09695*, 2025.

Qiying Yu, Zheng Zhang, Ruofei Zhu, Yufeng Yuan, Xiaochen Zuo, Yu Yue, Tiantian Fan, Gaohong Liu, Lingjun Liu, Xin Liu, et al. Dapo: An open-source llm reinforcement learning system at scale. *arXiv preprint arXiv:2503.14476*, 2025.

Tianyu Yu, Yuan Yao, Haoye Zhang, Taiwen He, Yifeng Han, Ganqu Cui, Jinyi Hu, Zhiyuan Liu, Hai-Tao Zheng, Maosong Sun, et al. Rlhf-v: Towards trustworthy mllms via behavior alignment from fine-grained correctional human feedback. In *Proceedings of the IEEE/CVF Conference on Computer Vision and Pattern Recognition*, pp. 13807–13816, 2024a.

Tianyu Yu, Haoye Zhang, Yuan Yao, Yunkai Dang, Da Chen, Xiaoman Lu, Ganqu Cui, Taiwen He, Zhiyuan Liu, Tat-Seng Chua, et al. Rlaif-v: Aligning mllms through open-source ai feedback for super gpt-4v trustworthiness. *arXiv preprint arXiv:2405.17220*, 2024b.

Chenshuang Zhang, Chaoning Zhang, Mengchun Zhang, and In So Kweon. Text-to-image diffusion models in generative ai: A survey. *arXiv preprint arXiv:2303.07909*, 2023.

Zhiyuan Zhao, Bin Wang, Linke Ouyang, Xiaoyi Dong, Jiaqi Wang, and Conghui He. Beyond hallucinations: Enhancing lmlms through hallucination-aware direct preference optimization. *arXiv preprint arXiv:2311.16839*, 2023.

Yiyang Zhou, Chenhang Cui, Jaehong Yoon, Linjun Zhang, Zhun Deng, Chelsea Finn, Mohit Bansal, and Huaxiu Yao. Analyzing and mitigating object hallucination in large vision-language models. *arXiv preprint arXiv:2310.00754*, 2023.

Yiyang Zhou, Chenhang Cui, Rafael Rafailev, Chelsea Finn, and Huaxiu Yao. Aligning modalities in vision large language models via preference fine-tuning. *arXiv preprint arXiv:2402.11411*, 2024a.

Yiyang Zhou, Zhiyuan Fan, Dongjie Cheng, Sihan Yang, Zhaorun Chen, Chenhang Cui, Xiyao Wang, Yun Li, Linjun Zhang, and Huaxiu Yao. Calibrated self-rewarding vision language models, 2024b. URL <https://arxiv.org/abs/2405.14622>.

---

## A EVALUATION

### A.1 HALLUCINATION REDUCTION INDEX

#### A.1.1 METRIC DESIGN

HRI represents an aggregate improvement metric across five different benchmarks. Simply summing the raw scores from each benchmark would not be a reasonable or rigorous approach, as the metrics are not directly comparable. Therefore, we calculate the improvement ratio for each benchmark based on its potential improvement range, effectively converting the raw metric gains into an additive proportion of improvement. Furthermore, we employ a conservative aggregation method to avoid overestimating the effectiveness of our approach.

Let  $a_i, i \in \{1, 2, 3, 4, 5\}$  denotes  $F1_{AMB-gen}$ ,  $Score_{MMHal}$ ,  $F1_{ObjectHal}$ ,  $LV_{score}$ ,  $F1_{AMB-dis}$  respectively, namely the results on each benchmark, superscript “ $base$ ” represents performances of the baseline model and “ $ref$ ” represents the set reference performances. Then HRI is calculated as:

$$HRI = 2 \times \sum_{i=1}^5 \frac{a_i - a_i^{base}}{a_i^{ref} - a_i^{base}} \quad (7)$$

#### A.1.2 MAIN RESULTS

For 7B model, we set the reference performances as  $OVIP_{2ep}$ , so it comes:

$$HRI = 2 \times \left( \frac{a_1 - 65.01}{67.12 - 65.01} + \frac{a_2 - 1.90}{2.65 - 1.90} + \frac{a_3 - 72.40}{74.18 - 72.40} + \frac{a_4 - 57.20}{60.90 - 57.20} + \frac{a_5 - 85.5}{87.4 - 85.5} \right)$$

For 13B model, we also use  $OVIP_{2ep}$  as the reference performances except for the ObjectHal benchmark which almost all methods fail to improve. We set the reference performance of ObjectHal to 79.0.

$$HRI = 2 \times \left( \frac{a_1 - 65.99}{68.98 - 65.99} + \frac{a_2 - 2.24}{2.57 - 2.24} + \frac{a_3 - 76.73}{79.00 - 76.73} + \frac{a_4 - 62.60}{67.90 - 62.60} + \frac{a_5 - 89.1}{90.2 - 89.1} \right)$$

#### A.1.3 ABLATION STUDY: LOSS FUNCTIONS

There is no method surpassing other methods significantly, so we consider the best performance on the benchmark as its reference performance.

$$HRI = 2 \times \left( \frac{a_1 - 65.01}{68.57 - 65.01} + \frac{a_2 - 1.90}{2.70 - 1.90} + \frac{a_3 - 72.40}{74.14 - 72.40} + \frac{a_4 - 57.20}{64.10 - 57.20} + \frac{a_5 - 85.5}{87.20 - 85.5} \right)$$

#### A.1.4 ABLATION STUDY: ONLINE AND OFFLINE

Same as Main Results.

$$HRI = 2 \times \left( \frac{a_1 - 65.01}{67.12 - 65.01} + \frac{a_2 - 1.90}{2.65 - 1.90} + \frac{a_3 - 72.40}{74.18 - 72.40} + \frac{a_4 - 57.20}{60.90 - 57.20} + \frac{a_5 - 85.5}{87.4 - 85.5} \right)$$

#### A.1.5 FURTHER STUDY

Same as Main Results.

$$HRI = 2 \times \left( \frac{a_1 - 65.01}{67.12 - 65.01} + \frac{a_2 - 1.90}{2.65 - 1.90} + \frac{a_3 - 72.40}{74.18 - 72.40} + \frac{a_4 - 57.20}{60.90 - 57.20} + \frac{a_5 - 85.5}{87.4 - 85.5} \right)$$

#### A.1.6 FAIRNESS

When aggregating different metrics through weighted averaging, it is necessary to account for the relative importance of each metric. Here, we define the potential improvement of a metric by considering its maximum observed gain in comparable experiments, and assign its weight as the inverse

---

of this gain to normalize across metrics. For example, if metric A shows a maximum improvement of 2 points while metric B improves by 4 points, we assume that an equally strong model would, on average, achieve only half as much gain on A as on B. Consequently, each point of improvement on A should be considered twice as important as a point on B. Compared with simple averaging, this weighting scheme better reflects the relative significance of different metrics and is less prone to being gamed.

## A.2 BENCHMARKS

- MMHal-Bench (MMHal) (Sun et al., 2024) is a model-evaluated question-answering benchmark covering 8 categories and 12 topics. While the original evaluation strategy uses GPT-4 to judge model responses, a text-only model will introduce considerable judging-time hallucinations and errors, so `gpt-4o-2024-05-13` is better for evaluation. (Amirloo et al., 2024).
- AMBER generative (AMBER<sub>gen</sub>) (Wang et al., 2023) is a judging-model-free benchmark for the image description task, comprising 1,004 samples. **Chair** measures the object-level hallucination rate as the average precision of objects mentioned in the model’s descriptions, while **Cover** indicates the recall of objects. *We observe a noticeable trade-off between these two metrics across various methods, where improvements in one often come at the expense of the other. To provide a more balanced and overall assessment, we introduce a new **F1** score calculated as the harmonic mean of Chair and Cover.*
- Object HalBench (ObjectHal) (Rohrbach et al., 2018) evaluates object-level completeness and hallucination rates. The generation prompts are augmented from Yu et al. (2024a). **Chair<sub>r</sub>** denotes the response-level hallucination rate. We also introduce an object-level **F1** metric to comprehensively measures the balance between hallucination and object coverage. Objects extraction is performed using `gpt-4o-2024-05-13`.
- Llava-Bench-in-the-Wild (LV) (Liu et al., 2023) evaluates models’ visual abilities, using 60 open-ended questions grounded in 24 diverse images from real-world and abstract scenarios. The evaluation is conducted using `gpt-4o-2024-05-13`.
- AMBER discriminative (AMBER<sub>dis</sub>) (Wang et al., 2023) includes 14,216 ‘Yes/No’ questions regarding objects in image. We use the **F1** score as its metrics.

## A.3 BAD CASES

### A.3.1 MMHAL

Shown in Figure 7, the original evaluation protocol utilizes the text-only `gpt-4-turbo-2024-04-09` to evaluate the model response, which has no access to the input image and can only infer from the given image contents and ground truth, so it will lead to many incorrect judgments. We replace it with `gpt-4o-2024-05-13`, which yields more accurate assessments.

### A.3.2 AMBER-GENERATIVE & OBJECTHAL

AMBER uses an automatic method for detecting the hallucination entity, which primarily relies on the pre-defined hallucination words. ObjectHal introduces LLM to extract the mentioned entities, its metrics are basically the same with AMBER. Figure 8 illustrates several cases of misjudgment in AMBER. Since the score is determined solely by the presence of specific predefined words rather than the actual semantic correctness, the hallucination rate (Chair score) is often overestimated. **Moreover, this issue becomes more pronounced as the diversity and informativeness of model responses increases.**

Many methods achieve great improvements in the Chair score (entity-wise hallucination rate), but often at the cost of a significant decrease in the cover rate (completeness and informativeness). Figure 9 provides an example of this information deficit phenomenon, which should also be considered in the evaluation of model performance.

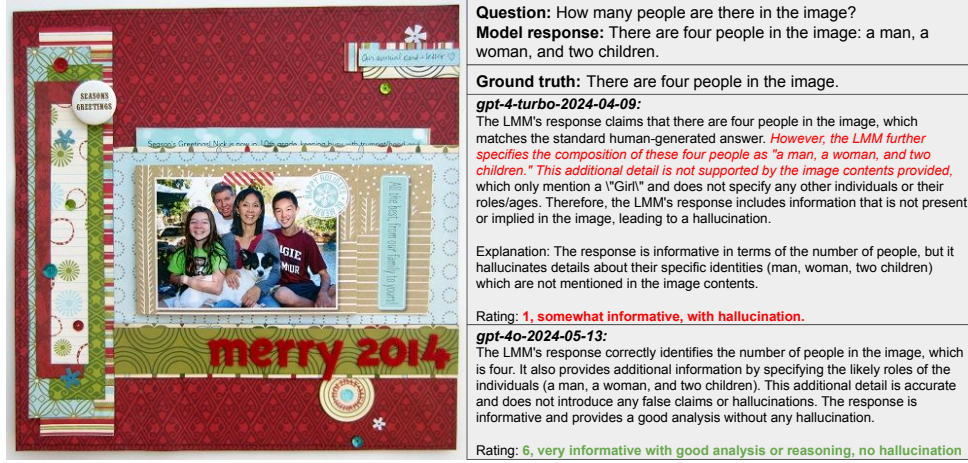


Figure 7: Text-only LLM can not correctly judge the response.

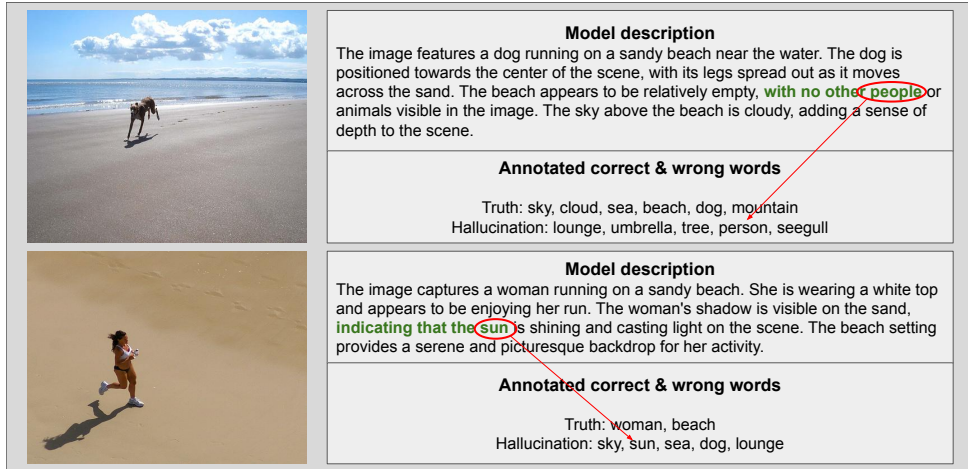


Figure 8: Rule-based extraction will lead to misjudgments to some extent.

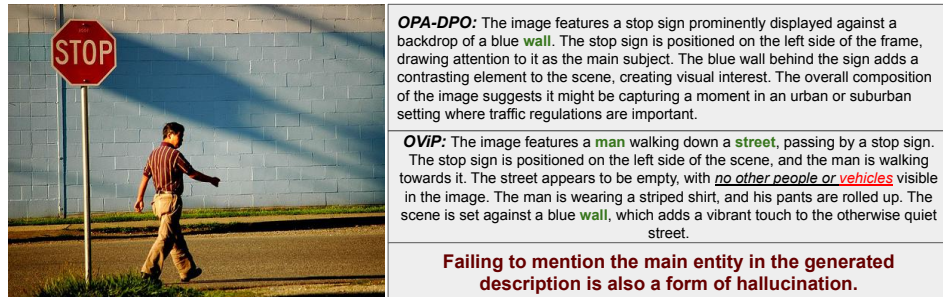


Figure 9: OPA-DPO fails to mention the man, a deficiency that is captured by Cover score but often overlooked in previous evaluations. “vehicles” is incorrectly identified as a hallucination word.

---

## B EXPERIMENTS

### B.1 LOSS FUNCTIONS

Base image loss  $\mathcal{L}_{\text{Image}}^{\text{base}}$  is similar to DPO loss which replace the response pair with the image pair:

$$\mathcal{L}_{\text{Image}}^{\text{base}}(\mathcal{I}^+, \mathcal{I}^-; \mathcal{Q}, \mathcal{A}^+) = \log \sigma \left( \beta \cdot \left[ \log \frac{\pi_\theta(\mathcal{A}^+ | \mathcal{I}^+, \mathcal{Q})}{\pi_{\text{ref}}(\mathcal{A}^+ | \mathcal{I}^+, \mathcal{Q})} - \log \frac{\pi_\theta(\mathcal{A}^+ | \mathcal{I}^-, \mathcal{Q})}{\pi_{\text{ref}}(\mathcal{A}^+ | \mathcal{I}^-, \mathcal{Q})} \right] \right)$$

Symmetrical image loss  $\mathcal{L}_{\text{Image-Sym}}$  considers the negative image and the negative response a correct pair, then calculate Image loss using negative response and image as the positive one:

$$\begin{aligned} \mathcal{L}_{\text{Image-Sym}}(\mathcal{I}^+, \mathcal{I}^-, \mathcal{A}^+, \mathcal{A}^-; \mathcal{Q}) = & \mathcal{L}_{\text{Image}}(\mathcal{I}^+, \mathcal{I}^-; \mathcal{Q}, \mathcal{A}^+) + \mathcal{L}_{\text{Image}}(\mathcal{I}^-, \mathcal{I}^+; \mathcal{Q}, \mathcal{A}^-) \\ = & -\log \sigma \left( \beta_1 \cdot \left[ \log \frac{\pi_\theta(\mathcal{A}^+ | \mathcal{I}^+, \mathcal{Q})}{\pi_{\text{ref}}(\mathcal{A}^+ | \mathcal{I}^+, \mathcal{Q})} - \log \frac{\pi_\theta(\mathcal{A}^+ | \mathcal{Q})}{\pi_{\text{ref}}(\mathcal{A}^+ | \mathcal{Q})} \right] \right. \\ & \left. + \beta_2 \cdot \left[ \log \frac{\pi_\theta(\mathcal{A}^+ | \mathcal{Q})}{\pi_{\text{ref}}(\mathcal{A}^+ | \mathcal{Q})} - \log \frac{\pi_\theta(\mathcal{A}^+ | \mathcal{I}^-, \mathcal{Q})}{\pi_{\text{ref}}(\mathcal{A}^+ | \mathcal{I}^-, \mathcal{Q})} \right] \right) \\ = & -\log \sigma \left( \beta_1 \cdot \left[ \log \frac{\pi_\theta(\mathcal{A}^- | \mathcal{I}^-, \mathcal{Q})}{\pi_{\text{ref}}(\mathcal{A}^- | \mathcal{I}^-, \mathcal{Q})} - \log \frac{\pi_\theta(\mathcal{A}^- | \mathcal{Q})}{\pi_{\text{ref}}(\mathcal{A}^- | \mathcal{Q})} \right] \right. \\ & \left. + \beta_2 \cdot \left[ \log \frac{\pi_\theta(\mathcal{A}^- | \mathcal{Q})}{\pi_{\text{ref}}(\mathcal{A}^- | \mathcal{Q})} - \log \frac{\pi_\theta(\mathcal{A}^- | \mathcal{I}^+, \mathcal{Q})}{\pi_{\text{ref}}(\mathcal{A}^- | \mathcal{I}^+, \mathcal{Q})} \right] \right) \end{aligned}$$

Anchor loss  $\mathcal{L}_{\text{Anchor}}$  directly enforces the probability of positive response to be higher for intuitively better optimization results.

$$\mathcal{L}_{\text{Anchor}}(\mathcal{A}^+, \mathcal{A}^-; \mathcal{Q}, \mathcal{I}^+) = -\log \sigma \left( \beta \cdot \log \frac{\pi_\theta(\mathcal{A}^+ | \mathcal{I}^+, \mathcal{Q})}{\pi_{\text{ref}}(\mathcal{A}^+ | \mathcal{I}^+, \mathcal{Q})} \right)$$

Bi-directional anchor loss  $\mathcal{L}_{\text{Bi-Anchor}}$  not only exerts supervision on the positive response, but it also makes the negative response probability to be lower.

$$\mathcal{L}_{\text{Bi-Anchor}}(\mathcal{A}^+, \mathcal{A}^-; \mathcal{Q}, \mathcal{I}^+) = -\log \sigma \left( \beta \cdot \log \frac{\pi_\theta(\mathcal{A}^+ | \mathcal{I}^+, \mathcal{Q})}{\pi_{\text{ref}}(\mathcal{A}^+ | \mathcal{I}^+, \mathcal{Q})} \right) + \log \sigma \left( \beta \cdot \log \frac{\pi_\theta(\mathcal{A}^- | \mathcal{Q})}{\pi_{\text{ref}}(\mathcal{A}^- | \mathcal{Q})} \right)$$

### B.2 SETTINGS

By default, we use the following settings:

**Software infrastructure.** In our implementation, we deploy the non-training LLM and diffusion models as services using FastAPI. During training, the system interacts with these services via API calls to obtain feedback, image prompts, and the paths to generated images.

**Models.** The LLM we use for judging response and providing image-generation prompt is `Qwen-2.5-7b-instruct` (<https://huggingface.co/Qwen/Qwen2.5-7B-Instruct>). The diffusion model for image generation is `FLUX.1-dev` (<https://huggingface.co/black-forest-labs/FLUX.1-dev>).

**Training** Both the 7B and 13B models are trained for a single epoch using a cosine learning rate schedule with a global batch size of 16. We set  $\beta = \beta_1 = \beta_2 = 0.1$  in Eq. 4 and Eq. 5. Learning rates are 1e-6 for 7B model and 5e-7 for 13B model.

**Sampling and Filter.** The score is between 0 and 10, which 10 means a perfect response and 0 means a totally incorrect response. We sample 16 responses for one query and set the lower-bound margin  $\delta$  to 3. Moreover, the quality criterion coefficients  $\tau_{\text{pos}} = \tau_{\text{neg}} = 5$ , which means the score of positive response should be at least 6 and negative response be at most 4. The **temperature** of the LLM scorer is 0.1.

---

Table 4: OViP pseudocode

---

**Algorithm 1** Algorithm of OViP

---

**Input:** training dataset  $\mathcal{D} = \{(\mathcal{I}^+, \mathcal{Q}, \mathcal{A}^*)\}$ ;  
 target model  $\pi$ ; reward model  $G_r$ ; prompt generator  $G_{\text{diff}}$ ; diffusion model  $\text{diff}$

**Initialize:** experience buffer  $\mathcal{B} \leftarrow \emptyset$

**Output:** optimized model  $\pi$

**for** each  $(\mathcal{I}^+, \mathcal{Q}, \mathcal{A}^*) \in \mathcal{D}$  **do**

- Sample candidate responses  $\{\mathcal{A}^i\}_{i=1}^k \sim \pi(\cdot | \mathcal{I}^+, \mathcal{Q})$
- Compute reward scores:  $r^i = G_r(\mathcal{A}^i, \mathcal{A}^*)$
- Compute standard deviation  $\sigma_r$  of  $\{r^i\}$
- Initialize temporary pair list  $\mathcal{T} \leftarrow \emptyset$
- while**  $\exists (\mathcal{A}^+, \mathcal{A}^-)$  satisfying:

  - $|r^+ - r^-| > \max(\delta, 2\sigma_r)$ ,  $r^+ > \tau_{\text{pos}}$ ,  $r^- < \tau_{\text{neg}}$  **do**
  - Add  $(\mathcal{A}^+, \mathcal{A}^-)$  to  $\mathcal{T}$  and remove from candidate pool

- end while**
- if**  $\mathcal{T} = \emptyset$  and  $\min_i r^i < \tau_{\text{neg}}$  **then**

  - Let  $\mathcal{A}^-$  be the lowest-scoring response
  - Add  $(\mathcal{A}^*, \mathcal{A}^-)$  to  $\mathcal{T}$

- endif**
- for** each  $(\mathcal{A}^+, \mathcal{A}^-) \in \mathcal{T}$  **do**

  - Generate prompt:  $\mathcal{T}^- = G_{\text{diff}}(\mathcal{A}^+, \mathcal{A}^-)$
  - Synthesize image:  $\mathcal{I}^- = \text{diff}(\mathcal{T}^-)$
  - Add  $(\mathcal{I}^+, \mathcal{I}^-, \mathcal{Q}, \mathcal{A}^+, \mathcal{A}^-)$  to buffer  $\mathcal{B}$

- end for**
- if**  $|\mathcal{B}| \geq N$  **then**

  - Sample  $N$  samples from  $\mathcal{B}$  for training
  - Compute total loss:  $\mathcal{L}_{\text{OViP}}$
  - Update  $\pi \leftarrow \pi - \eta \nabla_{\pi} \mathcal{L}_{\text{OViP}}$

- endif**

**end for**

---

Our hyperparameter settings are based on preliminary experiments and empirical intuition. We observe that when the model assigns a score between 0 and 3, the responses tend to contain significant errors, while scores of 7 and above generally indicate correct answers. The more strict the preference filtering criteria is, the higher the data quality tends to be; however, this also leads to fewer preference pairs satisfying the condition. Therefore, our choice of hyperparameters is based on a balance among empirical observations, data quantity, and data quality.

**Image Generation.** For image prompt generation, we set the model’s **temperature** as 0.1, **top\_p** as 0.9, and **max\_new\_tokens** as 128. We generate a  $384 \times 384$  image given the prompt with **num\_inference\_steps**=40 and **guidance\_scale**=7.5.

We perform ablation and further study using LLaVA-1.5-7B. The following describes the relevant experimental settings.

### B.2.1 ABLATION ON LOSS FUNCTIONS

We fine-tune the model for one epoch using data generated by the model itself immediately before training, following the OViP data construction pipeline.

Table 5: Online v.s. Offline detailed results

	Chair↓	AMB <sub>gen</sub> Cover↑	F1↑	MMHal Score↑	ObjectHal Chair <sub>r</sub> ↓	F1↑	LV Score↑	AMB <sub>dis</sub> F1↑
Baseline	7.1	50.0	65.01	1.90	51.38	72.40	57.20	85.5
DPO <sub>online</sub>	<b>4.7</b>	<b>50.0</b>	<b>65.59</b>	<b>2.38</b>	<b>31.58</b>	71.70	<b>56.10</b>	<b>86.7</b>
DPO <sub>offline</sub>	7.0	48.3	63.58	2.06	52.61	<b>72.55</b>	53.60	85.9
OViP <sub>online</sub>	<b>4.0</b>	<b>51.1</b>	<b>66.70</b>	<b>2.52</b>	<b>33.22</b>	<b>73.50</b>	<b>63.10</b>	<b>87.1</b>
OViP <sub>offline</sub>	5.2	49.9	65.38	2.35	46.34	72.39	60.20	86.6

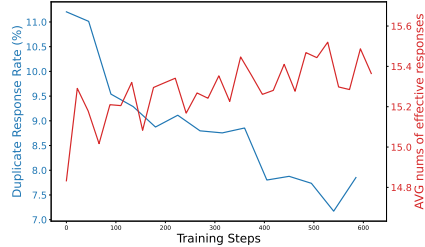


Figure 10: Sampling statistics during training. The blue curve shows the probability that, when sampling 16 responses with Temperature 1.2 for the same prompt, multiple identical responses appear (i.e., the number of distinct responses is fewer than 14). The red curve shows the average number of distinct responses obtained when sampling 16 times with Temperature 1.2.

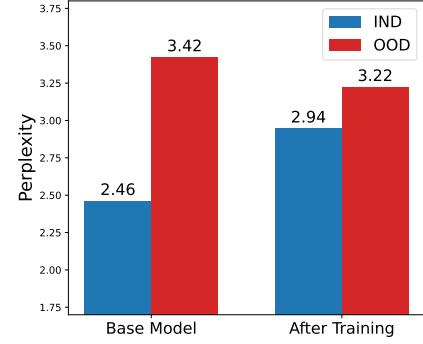


Figure 11: Perplexity changes for IND and OOD sequences. The perplexity of base model’s generation is relatively low.

For *iterative training*, we first fine-tune the base model on the original dataset using DPO to obtain a stronger initialization. We then sample and filter 4,730 instances as the second-stage contrastive dataset, which remains fixed across all variants. To improve supervision quality, model responses are annotated using DeepSeek-V3 for more accurate reward estimation.

### B.2.2 ABLATION ON ONLINE LEARNING

Although online methods can continuously improve when trained with another epoch, we conduct the experiment with one epoch for both online and offline methods.

## B.3 RESULTS

The training results for online and offline are shown in Table 5. Online training is significantly more effective in mitigating hallucinations.

### B.4 TRAINING DYNAMICS

The model’s initially skewed output distribution leads to a high rate of duplicate samples (in Figure 10, Duplicate Response Rate surpasses 11.0% at first) and very low perplexity Figure 11 in the generated responses, which is not conducive to optimization. In the early stages of training, the output distribution gradually flattens, but the limited exploratory scope prevents the model from identifying the correct optimization direction, resulting in stagnation of performance metrics. As the coverage of the distribution expands, the model can effectively explore the correct update directions, allowing training to get on track and performance to accelerate.

## C ALGORITHM

The pseudocode is at Table 4.

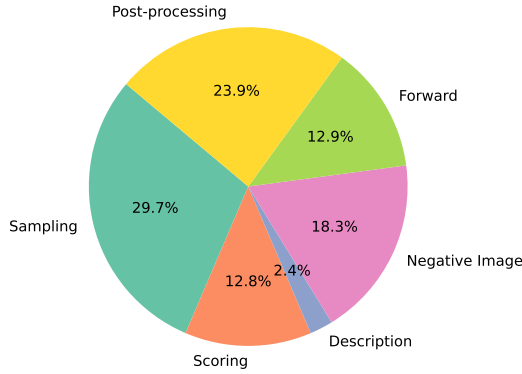


Figure 12: Time consumption for each stage during training.

## D EFFICIENCY AND TIME CONSUMING

OVIP training takes approximately 17 hours on 7× A800 (40G) GPUs. Among them, 4 GPUs are allocated for VLM training, 1 GPU for LLM deployment, and 2 GPUs for diffusion model deployment. We divide each training step into six stages: sampling (response generation), scoring (response evaluation), description (image prompt construction), negative image (counterfactual image generation), forward (model inference), and post-processing. Figure 12 illustrates the proportion of time spent on each stage, where post-processing refers to the period after forward propagation and before the next training step begins, including gradient accumulation, backpropagation, optimizer updates, and other related operations.

Excluding post-processing, the most time-consuming component is the sampling stage, similar to reinforcement learning. This is because it requires autoregressive generation of 16 responses, one token at a time. The second most expensive stage is negative image generation. To reduce latency, we parallelize this process by assigning two diffusion models to handle image generation requests from four sampling subprocesses.

Additionally, since the experience buffer is implemented independently in our system, repeated sampling by one subprocess may block others due to synchronization constraints. This can indirectly slow down the forward and post-processing stages as some processes await completion.

## E LIMITATIONS

This work introduces an online training framework that integrates dual contrastive learning across vision and language. While our loss function follows the DPO formulation, we do not explore how existing reinforcement learning algorithms—such as PPO or GRPO—could be effectively combined with image-level contrastive objectives. In terms of evaluation, although we identify and discuss several limitations of prior protocols and propose improved metrics and procedures, the current benchmarks still fall short of fully capturing model capability. We manually identified a subset of erroneous cases through inspection, but did not conduct a comprehensive correction. Lastly, our data filtering strategy during sampling has not been carefully tuned, and a more refined design could potentially lead to better training dynamics and model performance.

---

## F PROMPTS FOR JUDGMENT AND NEGATIVE IMAGE GENERATION

### Prompt for Quality Judgment

#### # Task

Your role is as a discerning assistant tasked with evaluating model responses for multi-modal tasks (though you have no access with the image). Upon being presented with a question that requires the interpretation of both text and images, you will receive two distinct responses. The first is crafted by our sophisticated multimodal model, while the second represents an approximate ideal answer—it may be incomplete. Your objective is to meticulously and precisely assess the model-generated response (the former) based on the provided reference answer (the latter).

- Here's how you should approach the assessment process:

1. The quality of the response depends on its accuracy and the degree of adherence to the correct answer. Therefore, if the response is much more detailed than the reference answer, it should not be considered a very good response (although it may still be considered a good one).

2. Directly provide the score of the response, with a full score of 10. Your response should follow this format: "Score: [x]\n", where "[x]" represents the score you give, and "\n" is a line break.

3. Please do not provide additional reasoning, just give the score directly.

#### # Question

{question}

#### # Response

{response}

#### # Correct answer

{answer}

Table 6: The prompt for judging model response given the answer.

## Prompt for image generation-Part 1

### # Task

Given an unknown image-related question, a correct answer, and an inaccurate response, carefully analyze the differences between the response and the answer. Then, provide a brief description of the image so that it aligns with the correct answer and differs from the incorrect responses. In other words, infer the content of the image.

### # Example

[Example 1]

\*\*<Question>\*\*

What is on the sandwich?

\*\*<Answer>\*\*

The sandwich has tomatoes and lettuce on it.

\*\*<Response>\*\*

The sandwich has a slice of egg and tomato on it.

\*\*<Output Description>\*\*

A sandwich with only tomatoes and lettuce on it.

\*\*Explanation\*\*: The answer mentions lettuce and tomato, while the incorrect response mentions tomato and egg. So there is no egg on the sandwich.

[Example 2]

\*\*<Question>\*\*

Can you point out the details that make this image unique?

\*\*<Answer>\*\*

In the image, there is a plate with a slice of pizza topped with tomatoes, herbs, and cheese. The distinctive detail about the image is that the pizza is missing two slices, leaving just one slice remaining on the plate. This suggests that someone has already started enjoying the pizza. The slice appears to be well-cooked and freshly served, creating an appetizing and mouthwatering scene for the viewer.

\*\*<Response>\*\*

In the image, there is a slice of pizza on a plate with tomatoes and cheese. The pizza appears to be homemade and has been cut into two pieces. The tomatoes are sliced in half, revealing their juicy interior. The cheese on top of the pizza is melted, creating a delicious-looking dish. Additionally, there is a fork nearby, suggesting that someone might be planning to enjoy this pizza soon.

\*\*<Output Description>\*\*

A plate with a one-third remaining piece of pizza, topped with herbs, cheese, and tomatoes; someone has finished eating and left.

\*\*Explanation\*\*: The answer mentions that only one-third of the pizza remains and that someone has just finished eating and left, which is inconsistent with the response. Therefore, the image should include these two features.

Table 7: The prompt for image generation.

---

### Prompt for image generation-Part 2

[Example 3]

\*\*<Question>\*\*

Bird or cow?

\*\*<Answer>\*\*

Bird

\*\*<Response>\*\*

The bird in the image is a small, brown and white bird with a distinctive head shape and coloration. It is not a cow. The bird is perched on a branch, which is situated in front of a white building.

\*\*<Output Description>\*\*

A big, blue bird perched on a branch in front of a black building.

\*\*Explanation\*\*: Both the answer and the response mention the bird, but the response is more detailed. So the description should be contrastive to the features of the bird in the response.

# Requirements

- The description should be brief but precise.
- If both the answer and the response are long, focus on describing the one or two most significant differences.
- Do not provide any analysis or explanation; only describe the image.
- A common approach is to describe what is present in the image and what is missing.

\*\*<Question>\*\*

question

\*\*<Answer>\*\*

answer

\*\*<Response>\*\*

response

\*\*<Output Description>\*\*

Table 8: The prompt for image generation.